WATER WASH INJECTOR ANALYSIS VIA
SIMULATION AND EMPIRICAL EVALUATION

K. J. Brown[*], W. Kalata, and R. J. Schick
Spraying Systems Co.
P.O. Box 7900
Wheaton, IL USA

Abstract

Petro-chemical refiners are required to move crude oil great distances throughout the refining process. Crude oil contains various salts which can lead to corrosion or plugging at various stages in the equipment. Water wash is often implemented to scrub the salts from the process stream to mitigate corrosion risks. Two modes of pipe degradation are addressed in this work: acid corrosion and erosion due to high wall shear stress.

The primary focus of this study is to define the distribution of injected water wash downstream of the injection point. This study builds on previous empirical and simulation studies that were performed with co-current spray operation by including counter-current and cross current injections. A hydraulic spray was investigated with a nominally uniform cross-flow air speed of 20m/s and 30m/s. These results demonstrate the trajectory change as well as the change in spray plume characteristics over a range of spray types and operating conditions, including counter-current and cross-current operation.

The experimental results were acquired with a LaVision Laser Sheet Imaging (LSI) and an Artium Phase Doppler Interferometer (PDI), to measure the spray shape, size, distribution characteristics as well as droplet size and velocity. The spray simulations were conducted using ANSYS FLUENT computational fluid dynamics (CFD) package in conjunction with custom spray injection methods developed in-house. Both steady-state and transient analysis was performed. The simulation work was also expanded to include transient phenomenon in the duct, such as secondary droplet breakup and improved particle-to-wall interactions.

---

[*]Corresponding author: Kathleen.Brown@spray.com

Introduction

Corrosion in the crude unit overhead plagues the refinery industry. It is a complex system that affects reliability, flexibility and the bottom-line. Process improvement and optimization in the refinery industry is a constantly ongoing effort.

The primary combatant of overhead fouling and corrosion is the desalter. The desalter is designed, under proper operation, to remove 90-98% of the water extractable chlorides that lead to corrosion issues and costly shutdowns [1].

Acid corrosion is one of the primary contributors to wall thinning in crude tower overheads. Acids in the vapor phase that pass through the desalter will transition to the water droplet, resulting in hydrochloric acid (HCl). The result is a low pH, highly corrosive liquid. HCl is formed when salts in crude hydrolyze under high temperature 160-380°C according to the following reactions [2]:

$$CaCl_2 + 2H_2O \rightarrow Ca(OH)_2 + 2HCl \ (\geq 204°C) \qquad (1)$$
$$MgCl_2 + 2H_2O \rightarrow Mg(OH)_2 + 2HCl \ (\geq 121°C) \qquad (2)$$
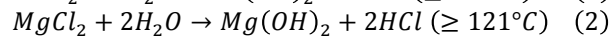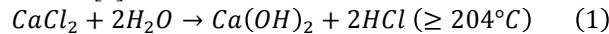
Most refiners use overhead water wash to force the condensation of water vapor. It is industry standard to use and additional 25% over the required flow, in order to dilute the acids that condense out with the water, further mitigating the corrosion risk.

The improvements made in nozzle design and liquid atomization in recent years have provided the possibility of process optimization like never before. In situ analysis would provide the best assessment of a spray's characteristics in a gas conditioning duct, however often this is cost prohibitive or not physically possible. Therefore, computational fluid dynamics (CFD) projects for this type of application have become very useful. With CFD, gas conditioning process engineers are able to, for the first time, assess the spray quality within the actual spray process region. The increased use of CFD to model these processes requires in-depth validation of the methods used to model these applications and the results provided by these types of models.

Spraying Systems Co. has the unique combination of testing and modeling expertise that allowed for a rigorous validation of these modeling techniques often used to simulate un-testable situations. This validation of computation fluid dynamics (CFD) results is wide reaching in applicable variables; the focus of the present study was on the relative type of the spray nozzle to a steady, nominally uniform co/cross-flow air stream. Various nozzle types and air speeds were assessed to determine optimal performance.

Technical Approach

Atomization of the injected water wash is key to controlling the condensation and evaporation of the water. Water droplets allow for evaporation and condensation to occur more readily than a flat surface. This curvature effect is shown in Figure 1[2].

Additionally, increased atomization increases the surface area contact with the gas phase. As drop size decreases, the surface area exposed to the gas phase increases rapidly. For example, the volume of one 500micron drop is equal to 121 x 100micron drops. The surface area of the 100 micron droplets is 484% larger than the surface area of the single 500 micron drop. Since mass transfer is proportional to the surface area of the drops, a small reduction in drop size can lead to significant improvement in mass transfer.

The second focus of this work was to improve distribution through the vapor stream. There are a plethora of sprays and orientations that can be used to inject water into a gas stream. Matching the spray characteristics to the gas stream is imperative to a successful application. In order for the spray to be effective the droplets must be carried a reasonable distance to allow for the mass transfer to occur.
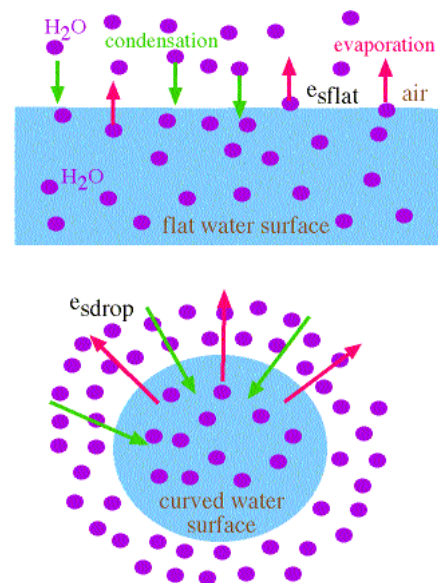

Figure 1. Curvature effect

Equipment and Methods

The experimental setup consisted of a spray nozzle, wind tunnel, PDI with traverse, and LSI system. All tests were carried out with the co-current and counter-current air flow. The injected fluid was liquid (water) at ambient temperature ~68°F. The nozzle was operated with a steady clean water supply for all tests as noted in Table 1. Injector type and direction schematics can be seen in Figure 2-3. In the interest of time, single full cone nozzles were not included in the Phase Doppler or simulation analysis.

Table 1. Injector Types & Operating Parameters

		Units	Case 1	Case 2	Case 3	Case 4	Case 5	Case 6
Injector Type			Hollow Cone	Full Cone	Dual Full Cone	Hollow Cone	Full Cone	Dual Full Cone
Nozzle ID			3/8BX-15	3/8GA-15	1/4HH-6.5	3/8BX-15	3/8GA-15	3/8HH-6.5
Air Flow Conditions		m/s	co-current 20-30	co-current 20-30	co-current 20-30	counter-current 20-30	counter-current 20-30	counter-current 20-30
Operating Pressure	ΔP	psi	135	137	195	135	137	195
Flow Rate	Q	gpm	5	5	2.5	5	5	2.5
Dv0.01	D_{min}	μm	7	15	58	7	15	58
Dv0.5	D_{mean}	μm	296	261	257	296	261	257
Dv0.9	D_{max}	μm	434	433	444	434	433	444
q			2.9	3.0	2.9	2.9	3.0	2.9

Wind Tunnel

The subsonic Wenham (blower-style) wind tunnel (shown in Figure 1) utilized in these experiments was capable of producing a co-current nominally uniform air flow at a velocity range from 2.5 m/s to greater than 50 m/s; the actual co/cross-flow velocity generated during these tests was 20 - 30 m/s. The wind speed was monitored and maintained using an upstream pitot tube arrangement. This wind speed was chosen as it allowed for a *reasonable* representation of the wash water injection systems commonly seen in the industry.

Figure 1. PDPA mounted with wind tunnel

Earlier work by Brown et al. [3] focused on the lower end velocities in the duct. In this expansion study, the velocity was slightly increased to allow within a normal operating range of the industry. These conditions are ideal for the inclusion of counter-current flow studies. Similar to past work, the characteristics of the spray plume was analyzed near the exit of the wind tunnel (location of wind tunnel optical access). Figure 1 provides an image

of the wind tunnel with a standard phase Doppler setup arranged around the test section; in these tests, the PDI system was oriented in a similar fashion with the addition of overhead traverse axes to allow for data acquisition at various y-locations.
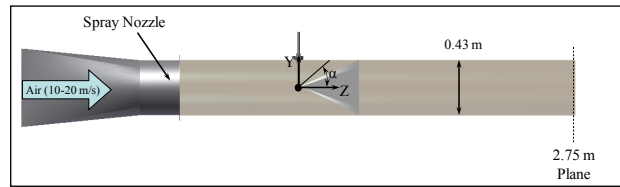


Figure 2. Wind tunnel coordinate system
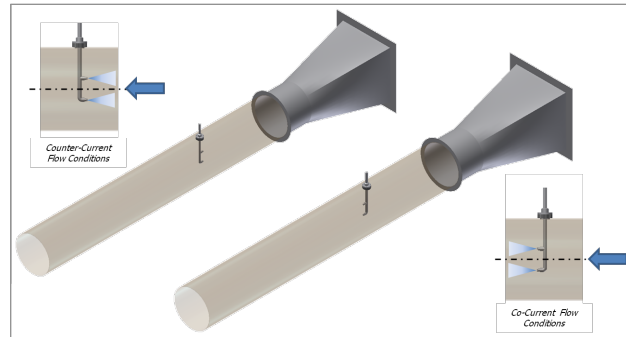
Figure 3. Flow Conditions

Figure 2 provides the wind tunnel coordinate system definitions for x, y, and z. The x-direction axis runs normal to the image with x=0 at the wind tunnel centerline; positive x is into the page. Flow direction was in the positive z direction for co-current flow. The direction of the injectors were rotated 180°, to simulate counter-current operation (Figure3). The single hollow cone, single full cone, and dual full cone options were evaluated by various mechanisms. Phase Doppler measurements and simulation activities were focused on hollow cone and dual full cone injectors with the effects of co-current and counter-current flow iteration.

Phase Doppler Interferometry

The phase Doppler Interferometry system used in this study was the Artium PDI 2D HD instrument with the integrated AIMS software used for automated processor setup. This technique measures the size, velocity, angle of trajectory, and time of arrival of each particle passing through an optical measurement volume formed by pairs of intersecting laser beams. The technical explanation of the Phase Doppler technique can be reviewed in a number of publications by Bachalo et al. [4,5]. The ability to measure accurately requires the reliable characterization of the size, velocity, and transit time of each droplet. The PDI system is a validated method for droplet size and velocity measurement; in addition, spray concentration measurements are possible, see Bade et al. [6].

The Artium PDI system utilizes a unique digital signal burst detection method which reliably detects droplets, even in complex environments. This is an advance over the earlier Fourier transform burst detection method invented by Ibrahim and Bachalo (U.S. Patent 5,289,391). This detection system is also critical to the in situ approach for measuring the effective diameter of the sample volume as a function of drop size. The Fourier transform based signal processor uses quadrature down-mixing to position the signals in an optimum range for processing. The real and imaginary (shifted by 90 degrees) components of the signals are sampled and a full complex Fourier transform is used to obtain the signal frequency and phase. Each of the three signals for the phase measurements is sampled in this manner and the phase differences computed at the same frequency for each signal. Three phase differences are computed, AB, AC, and BC for detectors A, B, and C from the Channel1 velocity component. These three phase differences are compared for consistency as one of the validations for each droplet signal detected. The approach has proven to be very effective in detecting and eliminating sizing errors due to the well-known trajectory problem.

The Artium AIMS software incorporates an *auto-setup* feature that serves to optimize the frequency and phase shift processing. The auto-setup feature acquires a small number of signals produced by droplets passing through the measurement volume and is discussed in detail in Bachalo, et al. [patent pending]. User-to-user setup differences that have been known to produce varying results and accuracy in PDI data results, often relying upon the operator's individual experience and understanding of the PDI principals, have been significantly minimized with this approach. The laser transmitting lens focal length was 500mm for all tests; the receiving unit focal length was 500mm for all tests and was oriented at the 40° off-axis forward scatter position. Masking was employed as necessary to provide an effective measureable drop size range of 10.6 to 584μm

(6.7 to 1349μm mask 2). Figure 1 illustrates the mounted traverse system around the wind tunnel test section, for these tests an Artium PDI was setup in a similar manner at the exit of the wind tunnel. Figure 4 demonstrates the experimental layout of the PDI system.
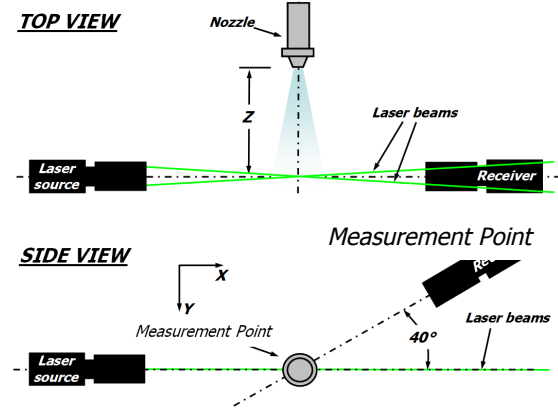

Figure 4. PDI system layout

Laser Sheet Imaging

The laser sheet imaging system implemented here was a commercial system developed by LaVision along with the associated DaVis image acquisition/processing software. The LSI system utilizes a laser sheet, with a Gaussian intensity profile, which illuminated the spray in a *single* downstream plane. The Gaussian intensity profile of the laser sheet is characterized and corrected for by imaging uniformly sizes fog droplets over the entire image area. The laser sheet was approximately 1mm thick which is sufficiently thin to represent a two dimensional sheet in the spray (z) direction, with images acquired in the x-y plane. The camera was located at an off-axis angle outside of the wind tunnel. The image calibration was conducted by first imaging a calibration-sheet with markings of know size and spacing to characterize and correct the skewed camera images to the actual planar spray cross-section plane. For these measurements the planar laser sheet was located at z=2.75m downstream of the nozzle location. This location was selected so that the spray attributes were noticeably well formed and wall impingement with the wind tunnel walls was complete.

In order to determine time averaged spray coverage and shape information. At each measurement, a minimum of 500 instantaneous (very short exposure time) images were acquired, and the average of all 500 planar intensity distributions was taken. It is important to note that the resultant mean images are representative of the average light intensity scattered, through Mie scattering, but droplets across the image plane. Over each image's exposure time, each droplet that passes through the laser sheet will scatter light relative to its surface area. On average, the two-dimensional contours are

therefore representative of the total surface area of droplets; which is a coupled result that is increased by an increase in the number of droplets and/or larger droplets. Ultimately, these results provide good information on the coverage and shape of the spray cross-section, and slightly less useful information on the surface area distribution, rather than a more used volume distribution, although there is good qualitatively relevant information. The LSI system was mounted to a custom fixture at the outlet of the wind tunnel system, similar to the Artium PDI setup, to allow for comparable data. Figure 5 illustrates the experimental layout of the LSI system.
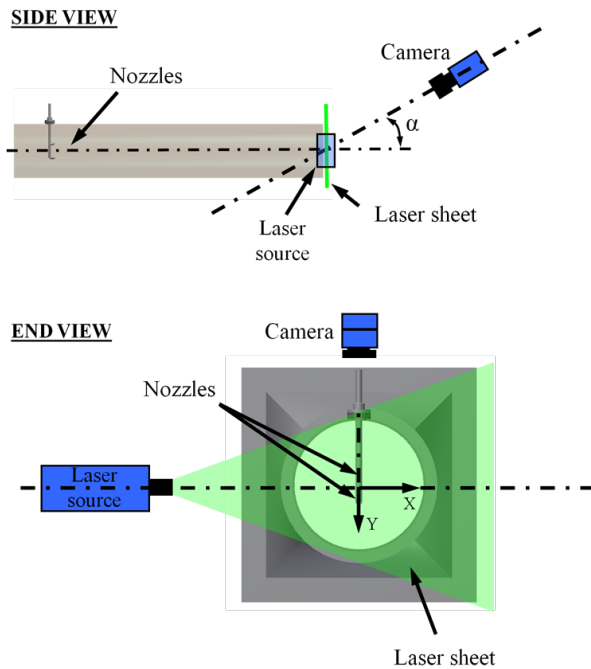
Figure 5. LSI system layout

Computational Setup and Methods

CFD simulations were performed with ANSYS FLUENT version 14.5. Generally, the CFD model was reproduced according to the wind tunnel geometry. The most significant alteration in the modeled geometry was the spray lance which was simplified to reduce the upstream mesh size. Meshing was performed within ANSYS Workbench using the automated meshing tool. Dense mesh was incorporated in the near vicinity of the spray injection locations. Size functions were used to further reduce mesh size. The 3D mesh consisted of mixed elements with approximately 2.0 million cells. Figure 6 provides a two-dimensional schematic of the CFD model setup and defines the coordinate system referenced in both the computational and experimental results.
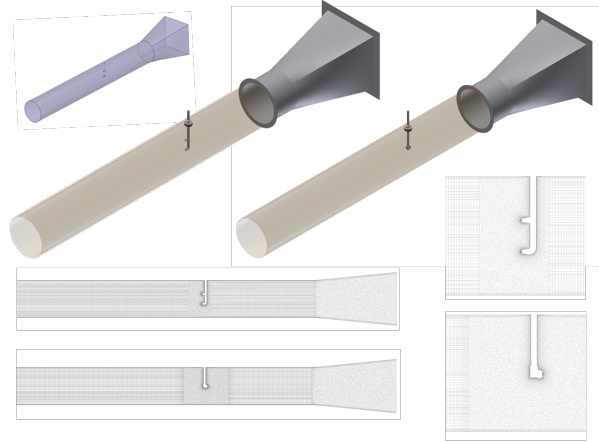

Figure 6. CAD model and CFD mesh detail

The CFD model was set up with a uniform velocity inlet boundary condition (BC) while varying the relative spray injection type and velocity magnitude in the duct. Figure 7 illustrates the nozzle types that were modeled and their orientation in the tunnel. Table 1 indicates the nozzle operating parameters and drop size parameters used for simulations. The outlet side of the duct was defined with a constant pressure boundary condition. The wind tunnel duct and lance walls were specified as rigid with no-slip and adiabatic conditions. Throughout all simulations the following models were included: k-ε Realizable Turbulence Model, DPM for LaGrangian tracking of water droplets, and Species Transport Model to include mixing of air and water vapor due to evaporation. Multiple turbulence models were evaluated to determine their suitability. The air phase and particle tracking were performed in steady state for most of the cases. The counter-current flow situations were evaluated with transient simulations to allow for the inclusion of secondary breakup as well as additional wall-settings.

The drop size distributions, exit velocity, and spray plume angle were obtained with PDI measurements in a vertical orientation at ambient conditions (no wind tunnel) and was used to define the CFD model spray injection parameters. The injection velocity was based on volume flux and area weighted averaged velocity at 10 mm downstream from the nozzle exit orifice, these weighing techniques are discussed in Bade et al. [6,7]. The minimum diameter (22 μm) input for CFD was specified based on volume flux and area weighted average of $D_{V0.01}$ and from the profile at 75 mm from injection. The maximum diameter (220 μm) for the CFD model was specified based on volume flux and area weighted average of $D_{V0.99}$ at the z=75mm downstream location (for drop size terminology see Lefebvre [8]). This process of combining the initial velocity characteristics and downstream drop size char-

acteristics was necessary in order to account for the lack of droplet collision and coalescence in the steady state model. The ANSYS Fluent input for drop size distribution was specified using the Rosin-Rammler distribution function, see Equation 3, to account for the 20,000 particles that were tracked at each iteration of the DPM model as discussed by Brown et al. [9].

$$Q = 1 - \exp\left(-\frac{D}{X}\right)^{q} \qquad (3)$$

Q is the fraction of total volume of drops with diameter less than D. X and q are constants inherent to the Rosin-Rammler function associated with the distribution center and width, respectively [8].

Spray Visualization Co-Current (DPM Conc. Results)

Hollow cone (3/8BX-15) - 30 m/s	Dual Full cone (1/4HH-6.5) - 30 m/s
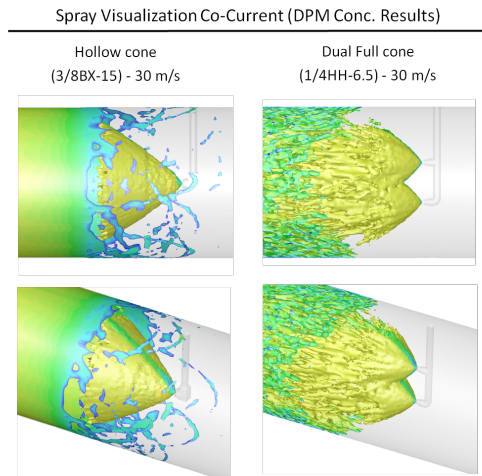
Figure 7. Injector Variation - Co-current

Spray Visualization Counter-Current (DPM Conc. Results)

Hollow cone (3/8BX-15) - 30 m/s	Dual Full cone (1/4HH-6.5) - 30 m/s
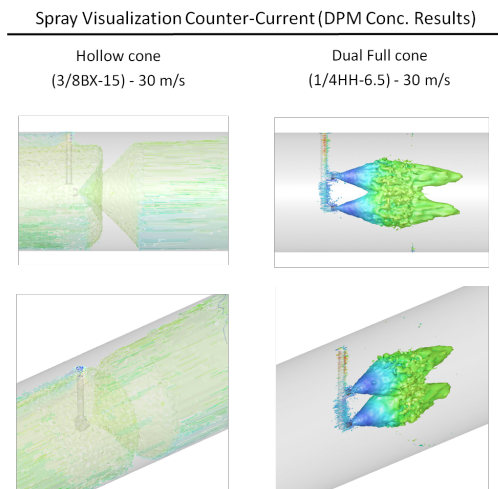
Figure 8. Injector Variation - Counter-current

Results and Discussion

PDI Results

While the LSI results provide a relatively qualitative assessment of the spray character, the PDI results provide the quantitative means for comparing the model to the experimental results. The drop size and velocity results at the z=2.75m location provide good insight to the effects of various injector types and air speeds. Figures 9-17 provide the PDI results at the downstream location.

Preliminary testing was done to aid in the selection of injectors with hollow cone, full cone and dual full cone plume shapes in ambient conditions, oriented vertically down. This allows for investigation of co-current flow, counter-current flow, and different injector types, with nearly identical spray performance inlet parameters.

In Figure 9, the effects of various nozzle types (relative to the purely co-current stream air flow) on the D_{32} distribution results are demonstrated. The hollow cone injector provides the widest distribution of droplets. Relatively course drop size is measured near the upper wall of the duct. Visually it is evident that this is due to a large amount of water attaching to the walls of duct. The bulk of the droplets measured at z=2.75m appear to be the result of liquid being stripped off of the duct. The absence of small droplets entrained in the gas stream, suggests that most of the volume injected into the domain impinge with the duct walls and form a film that travels down the duct.

The dual full cone nozzle provides the least variation in drop size across the measurement plane, at the z=2.75m location. As the measurement location is increased from the center of the duct, the D_{32} values increase at each positive y-location from the wind tunnel centerline (y=0). This trend follows the expected results and observed phenomenon in the duct. The extents of the data for both drop size and velocity results was set according to the existence of sufficient droplet concentrations (counts) to allow for *reasonable* data rates with the PDI, in general this acceptable rate was on the order 30 Hz or 30 droplets per second.

The trend for both cases are similar at the 20m/s and 30m/s air velocities investigated. For the hollow cone nozzle there is greater evidence of coating of the top of the duct. There is a significant impression of the top surface of the duct in the drop size data. This would indicate the formation of a liquid sheet on the duct and the separation of the sheet due to gravitational forces.

However, the effect on the dual full cone is more significant. The uniformity of the drop size is improved, as well as reduced overall. This would indicate a greater level of droplet entrainment. The overall reduction, though small, would indicate the occurence of secondary breakup.
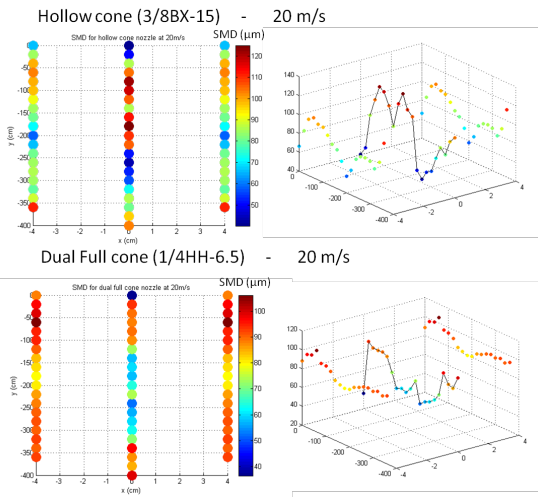
Figure 9. Drop Size at Co-current, 20m/s air speed
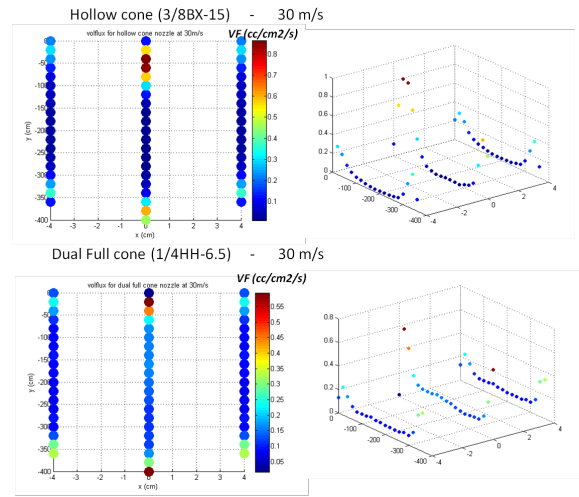
Figure 12. Volume Flux at Co-current, 30m/s air speed
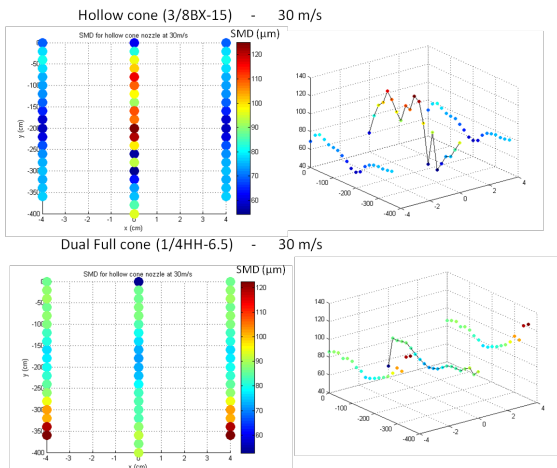
Figure 10. Drop Size at Co-current, 30m/s air speed
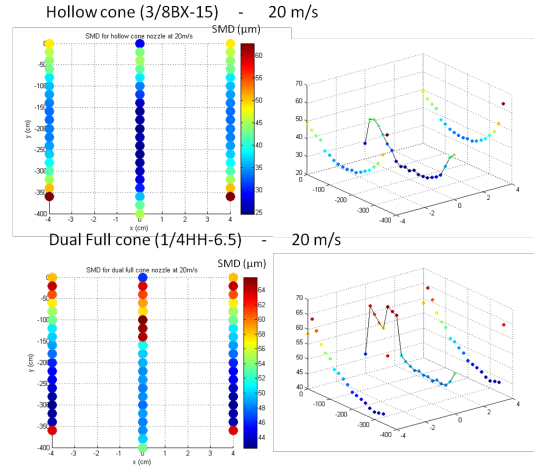
Figure 13. Drop Size at Counter-current, 20m/s air
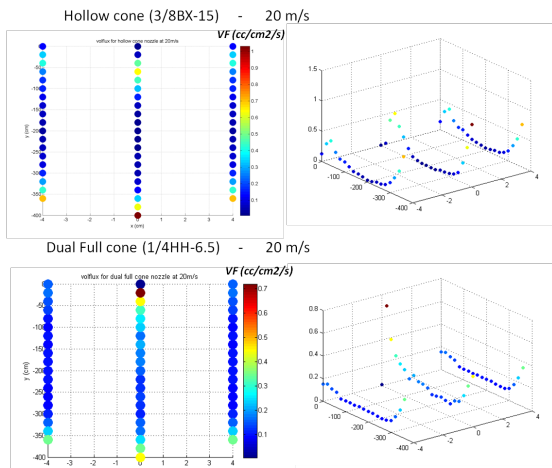
**Figure 11.** Volume Flux at Co-current, 20m/s air speed
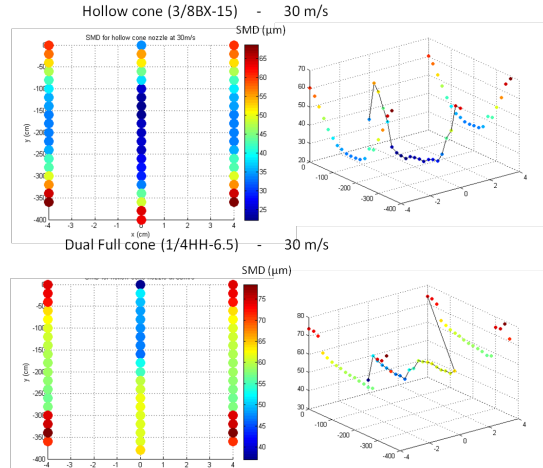
Figure 14. Drop Size at Counter-current, 30m/s air
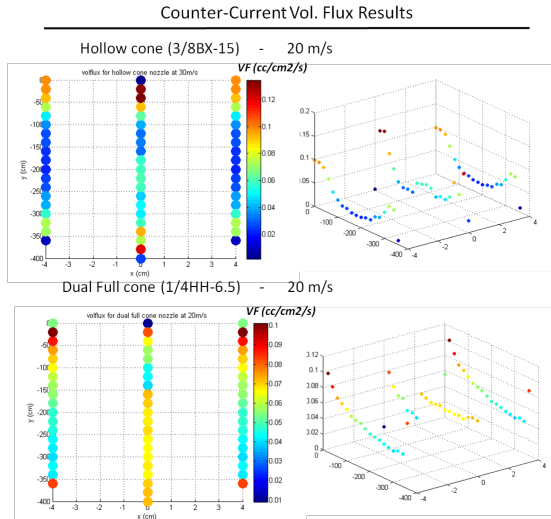
Figure 15. Volume Flux at Counter-current, 20m/s air
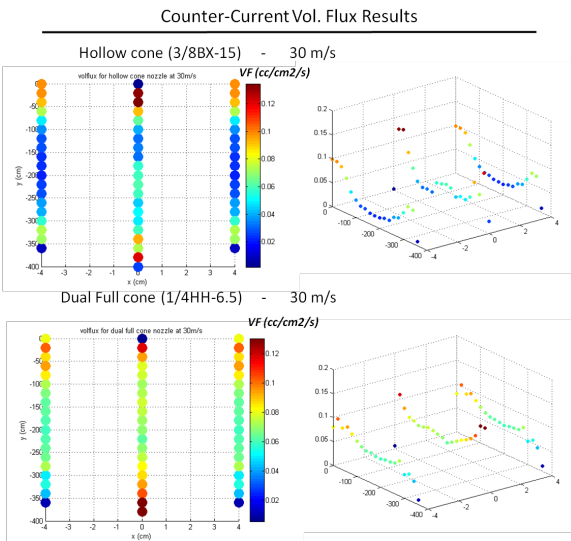
**Figure 16.** Volume Flux at Counter-current, 30m/s air
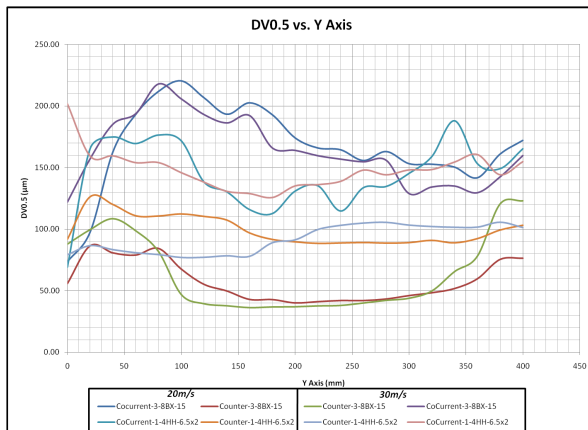
Figure 17. Drop Size - Center Profile

From examination of Figure 17, both injector types, speeds, and directional configurations can be compared. The most significant factor on drop size, is the direction of the air flow relative to the injection direction. The counter-current flow shows smaller droplet in the center of the plane. However near the edges of the duct, drop size increases dramatically. The dual cone outperforms the hollow cone style injector, by providing a consistenly smaller and more uniform entrained drop size distribution. The air speed consistently reduces the drop size. However the reduction is incremental and not significant enough to offset the cost of potentially reducing throughput or replacing the duct with an increased diameter.

LSI Results

The LSI results at both air velocities, with each injector, provide an impression of the spray liquid distribution at z=2.75 m; these 12 average images are provided in Figures 19-20. The overall spray shape represents a somewhat circular pattern. The hollow cone nozzle exhibits a clearly low concentration center with a slight vertical drop. There are two main factors influencing the determination of this shape. The direction of the droplets as they exit the nozzle, and the momentum of the droplets will determine the effect of the drag forces from the co-flowing air stream along with gravitational effects on the system. Due to the size of the droplets, the droplets exit the nozzle with significant momentum. The LSI results and visual observations verify that the momentum of the droplets far exceeds the air flow, hence there is little effect on the droplet trajectory of the hollow cone injector between the orifice and wall. This trend is repeated at both 20m/s and 30m/s.

The level of coverage in the measurement plane increases greatly from the hollow cone to dual cone injectors. Though the dual full cone exhibits smaller drop size, the momentum of the outer most droplets in not significantly altered by either the 20m/s or 30m/s air and is directed at the wall of the duct. Spray angle for each injector is reduced by less that 5% due to the air flow. A sample of the raw LSI image is contained in Figure 18. Figures 19 and 20 contain the corrected images for each injector, at 20m/s and 30m/s air speed, with co-current and counter current flow, respectively.
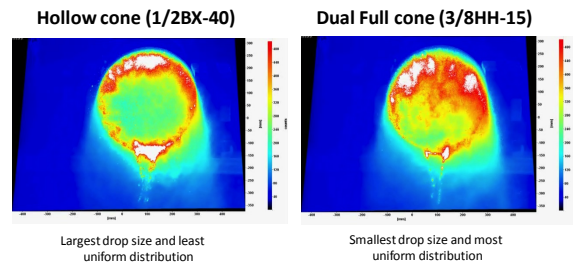

Figure 18. Raw LSI images
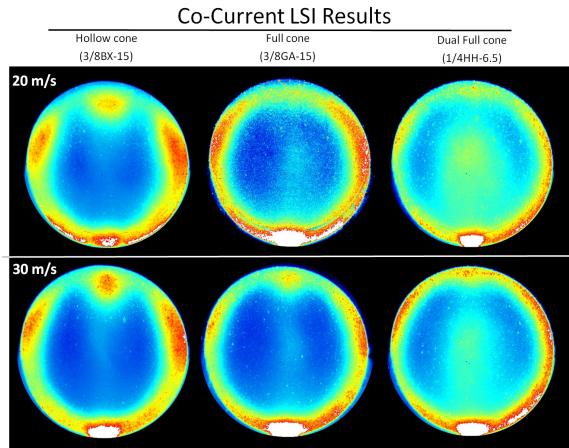
**Figure 19.** LSI Corrected images with co-current flow conditions
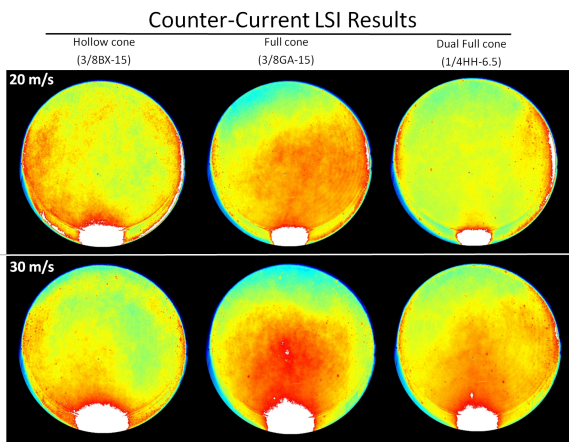
Figure 20. LSI Corrected with counter-current flow conditions

By comparison of Figures 19 and 20, the coverate of the co-current is consistently more uniform. However, in all cases there is a noticable film layer on the outer walls of the duct. Additionally there is a large amount of fluid running off of the bottom of the duct. This runoff is documented in Figure 21.
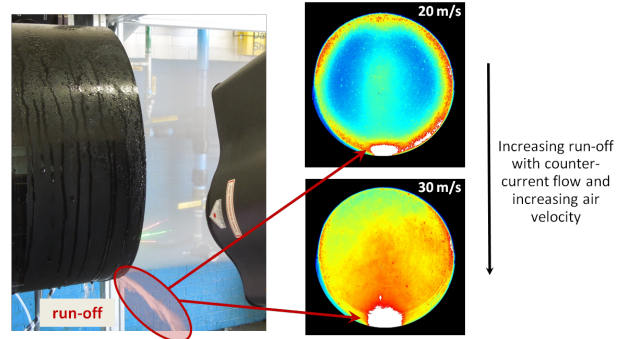

Figure 21. Evidence of Run-off observation and appearance in LSI Results

It is industry standard to inject 125% of required flow. Since the run-off was significant, the mass flow of the run-off was measured by a simple capture/weight method. The results of the run-off measurement are shown in Table 2. The trends support the visual results from the LSI testing.

Again the run-off was heaviest for the hollow cone and smallest for the dual full cone injectors. However, the effect the direction of the gas flow is more significant. The counter-current flow consistently resulted in the largest amount of run-off, and consequently results in the largest amount of waste. The counter-current trials resulted in 51-88% run-off. The uniformity of the drop size is smaller through the center of the duct, but the resulting waste far outweighs the benefit of reduced drop size.

The dual full cone has the best entrainment behavior exhibited. The desired overspray is provided by the dual full cone injector, with 30m/s of co-current flow. This hits the ideal industrial design specification. This co-incides with the most uniform drop size distribution combination as well.

CFD Results

The results from the CFD three-dimensional simulations are provided in order to show the distributions of drop size and velocity as well as the simulated trajectory of the droplets as they interact with the co-current

Table 2. Injector Types & Runoff

	Units	1	2	3	4	5	6	7	8	9	10	11	12
Injector Type		HC	FC	2xFC	HC	FC	2xFC	HC	FC	2xFC	HC	FC	2xFC
Nozzle ID		3/8B X-15	3/8G A-15	1/4H H-6.5	3/8B X-15	3/8G A-15	3/8H H-6.5	3/8B X-15	3/8G A-15	1/4H H-6.5	3/8B X-15	3/8G A-15	3/8H H-6.5
Air Flow Conditions		co-current			co-current			counter-current			counter-current		
Air Velocity	V	m/s	20	20	20	30	30	30	20	20	20	30	30	30
Operating Pressure	ΔP	psi	135	137	195	135	137	195	135	137	195	135	137	195
Flow Meter	Q_{TOTAL}	gpm	5.0	5.0	5.0	5.0	5.0	5.0	5.0	5.0	5.0	5.0	5.0	5.0
Runoff	Q_{TOTAL}	gpm	1.7	1.9	1.6	1.6	1.7	1.4	4.4	3.7	3.5	3.6	2.8	2.5
Runoff %		%	34	38	32	31	34	27	88	74	71	71	56	51

air stream. There is a very small degree of collapse of the spray plume, or reduction in spray angle. This demonstrates the effects of drag even when the primary droplet velocity is high relative to the co-current stream of the surrounding air. Additionally, this effect is slightly more dramatic with the 30m/s results which show the slightly more aggressive change in droplet trajectory due to the increased air flow condition.

In Figures. 22-25 the downstream planar spray shape can be seen. For all cases, the spray is nearly axisymmetric and circular, the drop diameters are highest outward from the center of the spray (most notable for the hollow cone spray). Spray distribution was also evaluated using the DPM concentration as a relative indicator of spray uniformity. In the following section, the CFD results will be compared with both types of experimental results (LSI and PDI) to draw conclusions regarding the results of each method and the driving causes of the spray characteristics.
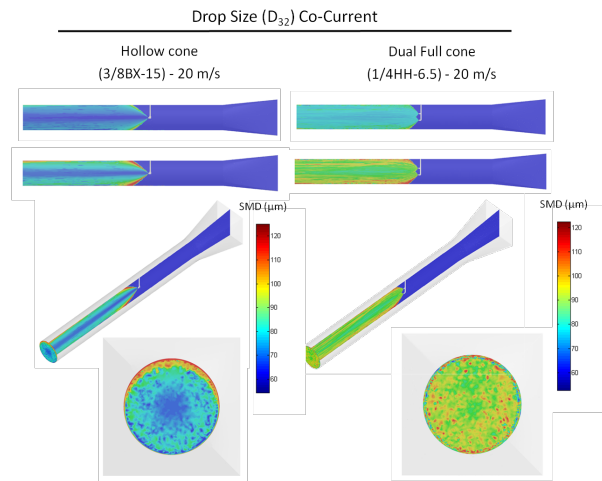

**Figure 22.** CFD Drop Size (D32) at 20m/s co-current flow
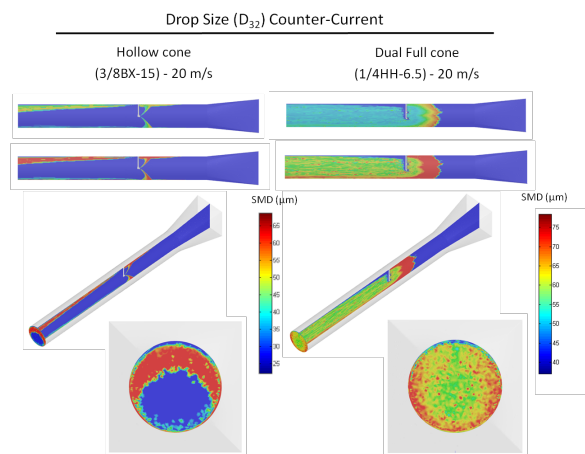
Figure 23. CFD Drop Size (D32) at 20m/s counter-current flow
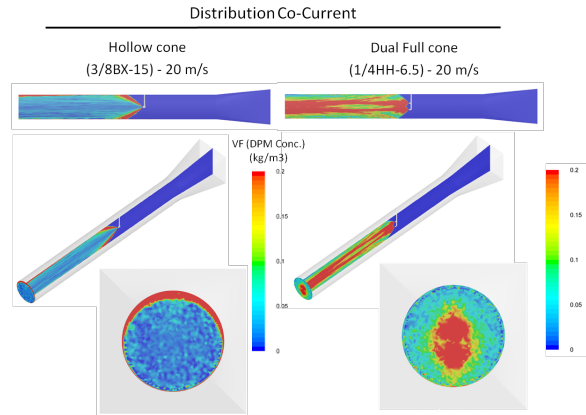

**Figure 24.** CFD Distribution (DPM Conc.) at 20m/s co-current flow
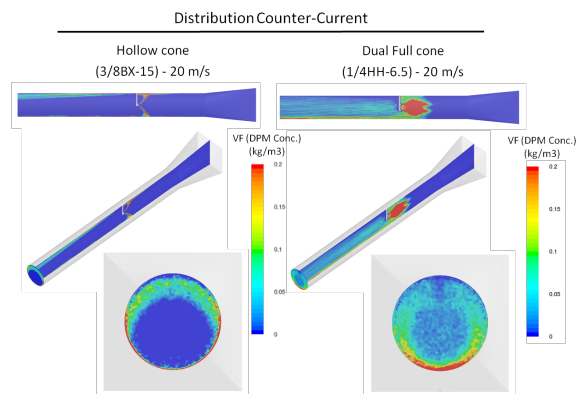
Figure 25. CFD Distribution (DPM Conc.) at 20m/s counter-current flow

Direct Comparisons and Conclusions

The comparison of experimental (LSI & PDI) and CFD results at z=2.75mm, for μ = 20m/s & 30m/s, demonstrates good agreement over the co-current flow orientation throughout the project. The comparisons are provided for wall wetting distance, spray uniformity, and D_{32}.

A comparison of the drop size (D_{32}) was examined for congruency. Figures 26 and 27 show the drop size comparison on identical scales. The trends in drop size are consistent from the PDI measurements to the CFD models. The hollow cone injector exhibits large drop size at the top of both the empirical measurements and the CFD model. However the model does not adequately capture the large drops and film at the bottom of the duct. Multiple wall boundary conditions were evaluated, with the results wall-jet boundary conditions shown. In all cases the wall conditions were found to be the focus of inaccuracies compared to the empirical results.

In a similar fashion, the dual full cone injectors provide good agreement with the PDI measurements, though the drop size of the model slightly overestimates

the drop size at the top of the duct. The model is adequate at replicating the increasing drop size near outer edges for the counter current configuration and larger drop size in the center region of the co-current configuration.
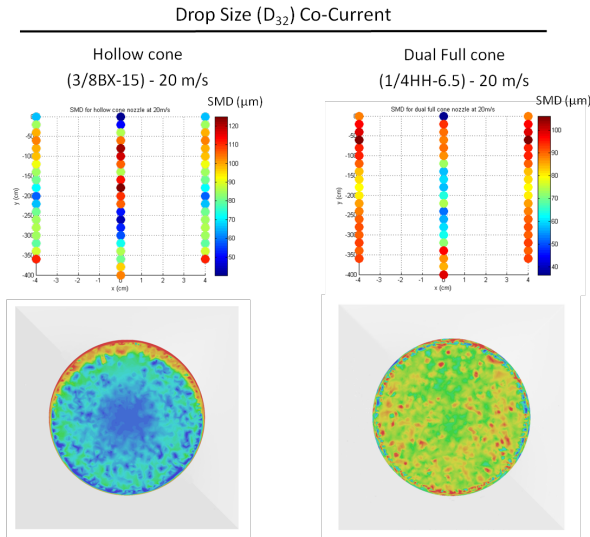


Figure 26. CFD / Empirical Drop Size Comparison
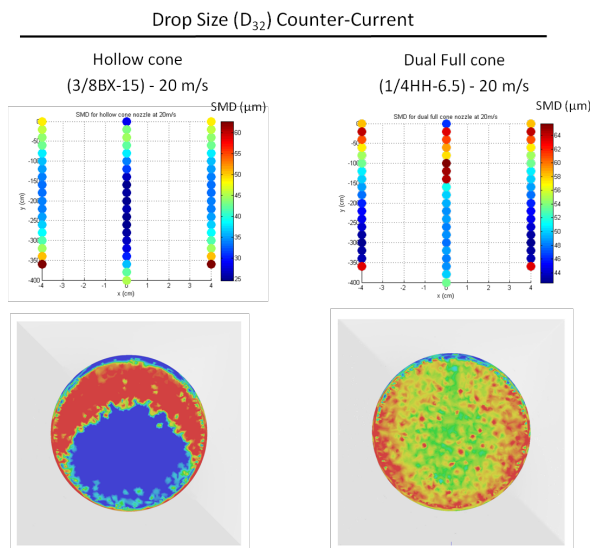
**Figure 27.** CFD / Empirical Drop Size Comparison
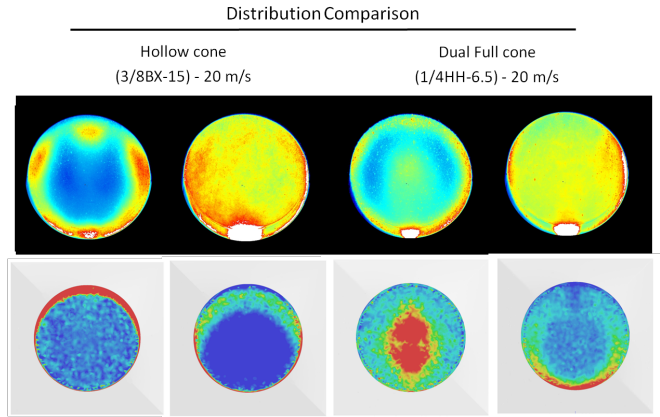
Figure 28. CFD Distribution (DPM Conc.) at 20m/s counter-current flow
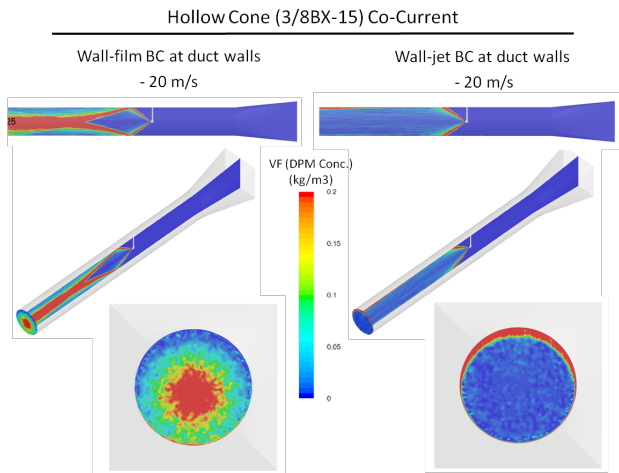

Figure 29. Comparison of wall boundary conditions

Multiple wall boundary conditions were evaluated, with the results wall-jet boundary conditions shown throughout. Wall film boundary conditions were also evaluated, with 4-8 splash settings. A sample of these results are shown in Figure 29. The difference in the results is considerable, with empirical results supporting the wall-jet boundary conditions. All steady state models fail to replicate accurately the film build up that contributes to the run-off. However examination of DPM concentration at the walls (with wall-jet), does provide a strong correlation to the observed areas of wall wetting.

Transient analysis was performed with the dual full cone, counter-current configuration. In transient mode, the wall-jet and wall-film provided more similar results. This would indicate that the wall-film model, though compatible with steady state analysis, is not recommended for steady state use in this type of application. Transient analysis is much more time intensive and thus less desirable for general use in projects with short timelines that are common for industrial design.

Conclusions

The experimental and computational results presented herein demonstrate good agreement in the spray characteristics over the range of injector types and gas flow parameters. These results demonstrate the validity of computational modeling which may be used in cases were experimental results are unavailable, cost prohibited, or impossible. Future efforts in this project are to include additional investigation of droplet to surface reactions. Additionally, the inclusion of measurements at various planar locations would be helpful to further validate spray performance.

Nomenclature

a acceleration
F force
m mass
ρ density

Subscripts

g gas
l liquid

Superscripts

$+$ downstream of the flame
$-$ upstream of the flame

References

1. Dion, M. et all., "Operating Philosophy Can Reduce Overhead Corrosion", Hydrocarbon Processing, March, 2012
2. Maddala, B.M. and Eid, M., "Corrosion Prevention, Protection & Control in CDU Overhead System", Proceeding of AIChE, 2008
3. Brown, K., Kalata, W., Schick, R.J.," Experimental and Computational Study of a Water Wash Spray Injection", Proceedings of ILASS 2013, May, 2013.
4. Bachalo, W.D. and Houser, M.J., "Phase Doppler Spray Analyzer for Simultaneous Measurements of Drop Size and Velocity Distributions," Optical Engineering, Volume 23, Number 5, September-October, 1984.
5. Bachalo, W.D. and Houser, M.J., "Spray Drop Size and Velocity Measurements Using the Phase/Doppler Particle Analyzer", Proceedings of the ICLASS (3rd Intl.), July 1985.
6. Bade, K.M., Schick, R.J., "Phase Doppler Interferometry Volume Flux Calculation Optimization and Comparison with Nominally Point Mechanical Patternation Techniques", Atomization and Sprays, vol. 21, no.7, pp537-551, 2011.
7. Bade, K.M., Schick, R.J., "Volume Distribution Comparison Methods for 1D, 2D, and Point Measurement Techniques", ILASS Americas 2008, Orlando, FL, May 2008.
8. Lefebvre, A. H., *Atomization and Sprays*, Hemisphere, New York, 1989.
9. Brown, K., Kalata, W., Schick, R.J.," Drop Size Distribution Analysis with respect to Height - Numerical Simulation versus Empirical Evaluation", Proceedings of ILASS 2008, May, 2008.

Acknowledgements